Local entanglement and confinement transitions in the random transverse-field Ising model on the pyrochlore lattice

Tom Pardini,[1] Anirudha Menon,[2] Stefan P. Hau-Riege,[1] and Rajiv R. P. Singh[2]
[1]*Lawrence Livermore National Laboratory, 7000 East Avenue, Livermore, California 94550, USA*
[2]*Department of Physics, University of California Davis, Davis, California 95616, USA*

(Received 31 July 2019; published 28 October 2019)

We use numerical linked cluster expansions (NLC) and exact diagonalization to study confinement transitions out of the quantum spin liquid phase in the pyrochlore-lattice Ising antiferromagnet with random transverse fields. We calculate entanglement entropies associated with local regions defined by single tetrahedron to observe these transitions. The randomness-induced confinement transition is marked by a sharp reduction in the local entanglement and a concomitant increase in Ising correlations. In NLC, it is studied through the destruction of loop resonances due to random transverse-fields. The confining phase is characterized by a distribution of local entanglement entropies, which persists to large random fields.

DOI: 10.1103/PhysRevB.100.144437

I. INTRODUCTION

In recent years, many candidate quantum spin-liquid (QSL) materials have been identified [1–7]. A characteristic of QSLs is the high degree of quantum entanglement, allowing them to host fractionalized quasiparticles. However, a convincing experimental demonstration of QSLs remains elusive. Part of the difficulty lies in the nature of the phase, which does not have a measurable order parameter. Emergent, fractionalized degrees of freedom do not directly couple to external probes. Thus, with few exceptions, such as the quantized thermal Hall effect [8], most experimental signatures of QSLs are indirect and subject to alternative interpretations. Impurities, which are ever present in condensed-matter systems, play a significant role in shaping the macroscopic phases, and understanding them is important for establishing a QSL experimentally [9–16].

One class of materials that have attracted significant interest are the spin-ice family of rare-earth pyrochlores [17–25]. Magnetic rare-earth ions form a lattice of corner-sharing tetrahedra. Though these ions typically have large spin, strong spin-orbit coupling and crystal-field effects map them onto an effective two-state or spin-half system. The local Ising axis is defined by the line joining the vertex to the center of the tetrahedron. When exchange interactions favor "2-in-2-out" Ising states in each tetrahedron, this leads to macroscopic ground-state degeneracy classically with the well-known Pauling entropy [26]. This classical spin-liquid, also called spin-ice, is well established in some rare-earth pyrochlores [18].

These materials can be divided into Kramers and non-Kramers systems [17]. The former consist of an odd number of electrons per ion, which must have a twofold degeneracy for every single-ion eigenstate. The latter will typically have nondegenerate eigenstates, and double degeneracy can only arise as a result of some lattice symmetry. Thus spin-active non-Kramers systems can arise from two nearby nondegenerate states well separated from the rest, or from a lattice-symmetry protected doublet ground state that will be split by impurities. These systems can be modeled by random-transverse field Ising models [27–32]. Indeed, the material $Pr_2Zr_2O_7$ is a realization of this model [33].

Here we study the quantum Ising antiferromagnet on the pyrochlore lattice by numerical linked cluster (NLC) expansions [34–36] and exact diagonalization (ED). We focus on the local entanglement properties of the system and examine their behavior at the confinement transitions. We find that entanglement of spins of a tetrahedron with the rest of the system contains sharp changes associated with different confining transitions.

A simple NLC calculation diverges inside the QSL phase. To obtain convergent results, one must consider each cluster as embedded in a superposition of spin-ice states. The confinement transition can be observed by studying the destruction of ring-exchange resonance due to the random fields. A modification of Benton's perturbative argument [28] shows that at the phase boundary the width of the transverse-field distribution scales quadratically with the mean value in agreement with the NLC results. We also find that the confining phase [32] is characterized by a broad distribution of local entanglement entropies, a property that persists to high random fields. This means that even with increasing random fields, there will be pockets of strong entanglement with local behavior of a QSL.

II. MODELS AND METHODS

We consider the Hamiltonian

$$\mathcal{H} = J \sum_{\langle i,j \rangle} \sigma_i^z \sigma_j^z - \sum_i h_i \sigma_i^x, \tag{1}$$

where $J = 1$, and the transverse fields h_i are independent Gaussian random variables with mean h and standard deviation w. On a finite cluster with periodic boundary conditions, we calculate the ground-state wave function of the system. We divide the system into two parts: A and its complement B. Let the reduced density matrix of A be ρ_A. The von-Neumann

entanglement entropy between A and its complement B is

$$S_A = S_B = -\operatorname{Tr} \rho_A \ln \rho_A. \tag{2}$$

In this work, A is made up of the four spins belonging to any single tetrahedron, and B is made up of all the remaining spins. This leads to the definition of single-tetrahedron entanglement entropy,

$$S_T = [-\operatorname{Tr} \rho_T \ln \rho_T]. \tag{3}$$

The square brackets indicate that the quantity is averaged over the tetrahedra in the cluster and over disorder configurations. In addition, we study the average moment along the local field, defined as

$$m_x = \left[\frac{1}{N} \sum_i \left| \langle \sigma_i^x \rangle \right| \right]. \tag{4}$$

Here N is the number of sites, and the angular brackets throughout this study refer to ground-state expectation values, while the square brackets refer to an average over disorder configurations. We also calculate the correlation sum for the Ising components:

$$C_{zz} = \left[\frac{1}{N(N-1)} \sum_{i,j \neq i} \left| \langle \sigma_i^z \sigma_j^z \rangle \right| \right], \tag{5}$$

where the sum is over all pairs of spins.

To obtain the results in the thermodynamic limit, we turn to the NLC [34–36]. An extensive property of interest P, per site, can be calculated by a sum over connected clusters c that can be embedded in the lattice.

$$P/N = \sum_c L(c) \times W(c), \tag{6}$$

where $L(c)$ is the lattice constant of the cluster, or the number of times the cluster arises in the lattice per site. The weight $W(c)$ is defined recursively as

$$W(c) = P(c) - \sum_s W(s), \tag{7}$$

where $P(c)$ is the property for the cluster, and the subtraction is over subclusters.

To study the property of spin-ice systems, it is useful to consider clusters made up of full tetrahedra [37,38]. To fifth order, i.e., up to five tetrahedra, there are a total of eight clusters. We include a ninth cluster, consisting of six tetrahedra in a ring, shown in Fig. 1, as it plays a special role in the spin-ice phase.

III. RESULTS AND DISCUSSION

We begin with results for the uniform system ($w = 0$). In Fig. 2, the expectation value of the spin along the transverse field and the local entanglement entropy associated with a single tetrahedron are shown as a function of the field. The fourth- and fifth-order NLC results are indistinguishable in the plot in the high-field paramagnetic phase, showing that they represent the results in the thermodynamic limit. The ED results for 16- and 32-site clusters are also shown. In the thermodynamic limit, there may be a small discontinuity

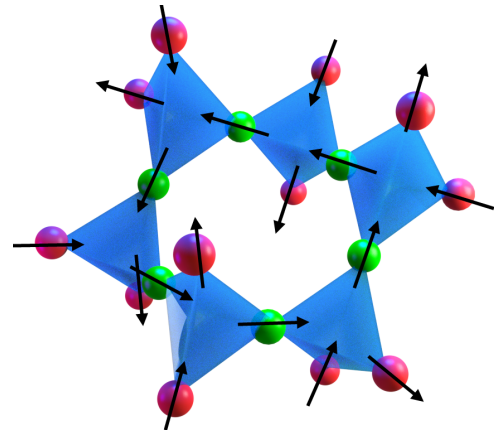

FIG. 1. Cluster of six tetrahedra connected in a ring. The six interior sites of the cluster are denoted by green circles, and the 12 boundary sites are denoted by red circles. The arrows denote one spin-ice configuration for the cluster.

at the transition [30,31], but finite-size effects are small in the paramagnetic phase right down to the transition. This first-order transition point from previous studies [30,31] is indicated by the vertical black lines.

While the simple NLC converges well in the high-field phase right up to the transition, it diverges in the QSL phase and we need to modify it for the QSL. The physics of QSL is lost by having fluctuating spins at the boundary of the finite clusters. This is because every spin must be part of two tetrahedra in order not to mix different ice states by local fluctuations. But the boundary spins of a cluster belong to only one. Thus, two boundary spins in the same tetrahedron can be flipped to go from one ice configuration to another already in order h^2. This is clearly incorrect.

To fix this problem, we adopt a modified NLC scheme. We envisage local fluctuations in the interior of the QSL. Each cluster is divided into interior and boundary spins depending

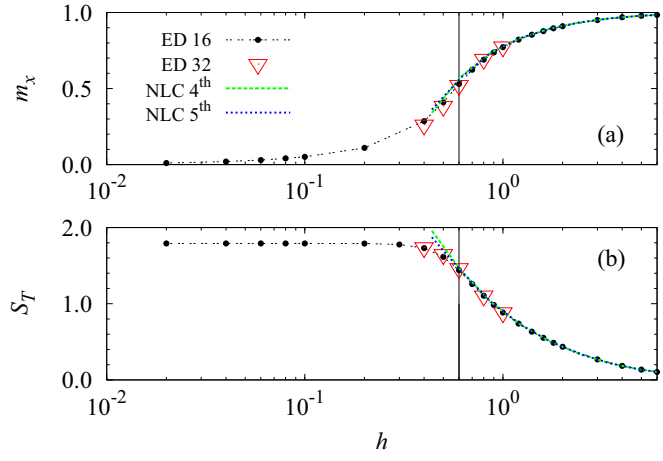

FIG. 2. (a) Expectation value of spin along the transverse field m_x, and (b) single-tetrahedron entanglement entropy S_T, as a function of the transverse field h with no disorder. The data are for 16- and 32-site clusters and fourth- and fifth-order NLC. The vertical black lines denote the transition point [30,31] between QSL and the paramagnetic phase. NLC does not converge within the QSL phase, and for this reason NLC results are not shown for small h values.

on whether the spin belongs to two or one tetrahedron in the finite cluster (see Fig. 1). The boundary spins feel additional longitudinal fields, coming from tetrahedra external to the cluster. It can be shown that the modified NLC in fifth order gives perturbative properties correct to order h^8 except for the ring exchanges. However, these perturbative terms generate very small entanglement at small fields, and ring exchanges are key to the physics of the QSL [21–23].

To capture the physics of ring exchanges, one must consider clusters where tetrahedra form rings. All the order-1 entanglement for small h arises from ring exchanges [23,30]. This resonance can be destroyed by random fields, effectively killing the superposition and consequential entanglement. For studying this, cluster 9 consisting of six tetrahedra in a ring shown in Fig. 1 plays a crucial role.

In this cluster, each tetrahedron has two interior and two boundary spins. In our modified NLC, the cluster is embedded in a larger system. The Ising couplings of the spins external to the cluster result in longitudinal fields on the boundary spins of the cluster. The problem is divided into different sectors corresponding to different boundary longitudinal fields. The key sector is one where in each tetrahedron one boundary spin has a positive and the other a negative longitudinal field. At low energies, this sector maps onto an effective two-level system given by the two alternating spin configurations along the hexagon of the cluster.

For a uniform system, this leads to an entanglement entropy for each tetrahedron of $\ln 2$ in the sector where the resonance occurs, and zero in all other sectors apart from small perturbative corrections. Thus a sum over all tetrahedrons gives $6 \ln 2$ in the resonating sector. The cluster has 730 total spin-ice states, 128 of which lead to the resonating state. If we assume that each one of the spin-ice states must be weighted with equal probability in the interior of the spin-ice as expected at the Rokhsar-Kivelson (RK) point [39], the weight of this cluster for the entanglement entropy per tetrahedron becomes $(6 \times 128/730)\ \ln 2$. This cluster has a count of one per site or two per tetrahedron. Thus, multiplying the weight by a factor of 2 gives an entanglement entropy for a tetrahedron in the thermodynamic system to be approximately 1.5. Our ED estimate for the low-field entanglement entropy shown in Fig. 2 is less than 20% higher than this. The comparison suggests that the resonating configurations are enriched relative to others by less than 20% with respect to the RK point in the model. This is consistent with the Monte Carlo study of the ring-exchange model [23].

We now turn to the main focus of our study with random transverse fields. The Ising correlation sum and tetrahedron entanglement entropy from ED are shown in Fig. 3, where we see that an increase in the Ising correlation occurs concomitant with a decrease in local entanglement entropy. This shows that the confinement transition is associated with the lifting of degeneracy in the spin-ice subspace and leads to the development of Ising correlations [32]. Figure 4 shows the distribution of single-tetrahedron entanglement entropies. One finds that as soon as one enters the confining phase, the entanglement entropy develops a broad distribution. Figure 4(b) shows a few cuts through the distribution function. In the QSL phase,

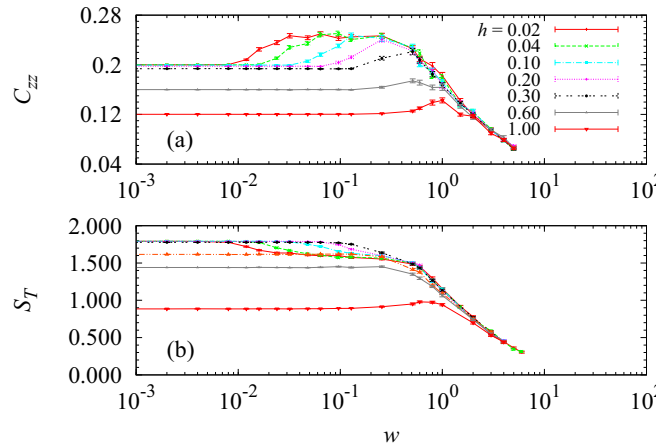

FIG. 3. (a) Ising correlations C_{zz}, and (b) single-tetrahedron entanglement entropy S_T as a function of width of the field distribution w for different mean values of the field h. Data have been obtained via ED on a 16-site cluster, and each data point represents an average over 100 independent disorder configurations. Error bars are from a finite sampling of disorder.

the entanglement entropy is essentially a δ function. In the confining phase it is broad. For the finite system, there remains weight at the largest value until one gets into a paramagnetic phase around $w = 0.5$, after which the peak gradually moves to smaller values. However, the distribution remains broad all the way up to large randomness. Existence of long range spin-glass order may lead to further reduction in entanglement. This deserves further attention.

Note that ED cannot give the correct thermodynamic phase boundary because our cluster has loops of length 4 coming from periodic boundary conditions. These small loops lead to a phase boundary where w scales linearly with h.

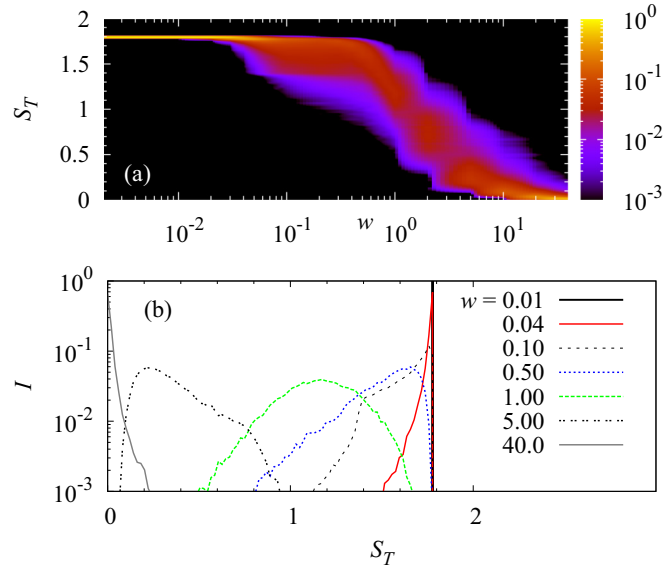

FIG. 4. (a) Distribution of single-tetrahedron entanglement entropy S_T for $h = 0.1$ and various w values. The color scale represents the normalized intensity I. (b) Several cuts of the intensity I in (a) for selected w values. For $w = 0.01$, the intensity is a δ function shown as a solid black line at $S_T \sim 1.77$.

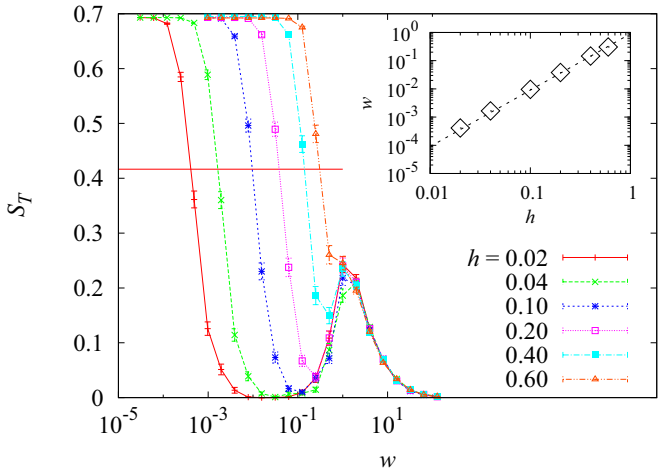

FIG. 5. Single-tetrahedron entanglement entropy S_T obtained from cluster 9 as a function of width w for different h values. Each data point represents an average over 200 independent disorder configurations. The horizontal line corresponds to $S_T = 0.4165$. The inset shows the transition point obtained from these calculations (diamonds) and from perturbation theory (dashed line).

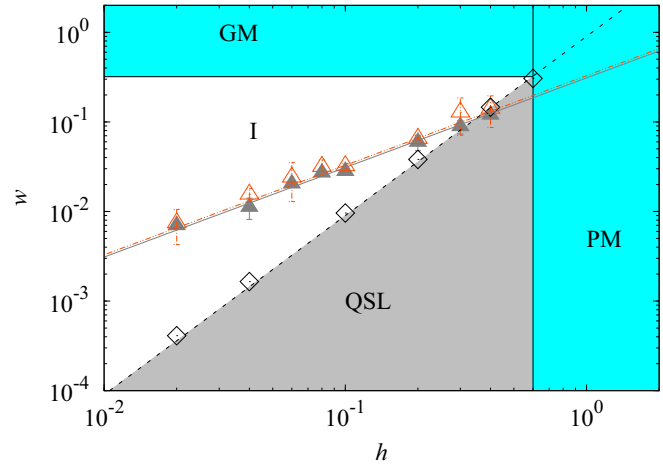

FIG. 6. A sketch of the phase diagram for the random transverse-field Ising model with QSL, paramagnetic (PM), Ising (I), and Griffiths-McCoy (GM) phases. The triangles represent a confinement phase boundary on the finite cluster. The diamonds are obtained from NLC and represent the phase boundary in the thermodynamic limit.

To study the phase boundary for the thermodynamic system, we must use NLC and focus on cluster 9. The tetrahedron entanglement entropy in the resonating sector of cluster 9 is shown in Fig. 5. We see that the resonance, which leads to an entanglement of ln 2, is killed with disorder. To further understand this, we turn to perturbation theory [28]. With disorder, the two-state problem for the cluster can be described by an effective Hamiltonian

$$H_{\text{eff}} = a\sigma_x + b\sigma_z, \tag{8}$$

where $a = \frac{63}{256}h^6$, while

$$b = \frac{1}{48}\sum_t \left(h_{i1}^2 - h_{i2}^2\right)\left(h_{b1}^2 - h_{b2}^2\right), \tag{9}$$

where the sum is over all six tetrahedra. Here, h_{i1} and h_{i2} are the random fields at the interior sites, and h_{b1} and h_{b2} are the random fields at the two boundary sites of the tetrahedra. Benton had argued [28] that the average degeneracy lifting perturbation should scale as wh^3. However, as seen from Eq. (8), there are two cancellations in each tetrahedron and b must vanish as w^2. We find that for Gaussian disorder it scales approximately as $14.7w^2h^2$. Calling the point $a = b$ the transition point gives the phase boundary $w = ch^2$, with $c \approx 0.90$. This phase boundary is also shown in the inset of Fig. 5 and agrees well with our calculations, where the transition is determined by the horizontal dashed line corresponding to an S_T of 0.4165 as appropriate for $a = b$ in Eq. (7).

A sketch of the phase diagram is shown in Fig. 6 with QSL, paramagnetic (PM), Ising (I), and Griffiths-McCoy (GM) phases. The Ising phase is characterized by enhanced random Ising correlations, whereas the Griffiths-McCoy phase is characterized by only pockets of entanglement corresponding to rare regions in the disorder configuration. The PM-QSL boundary is indicated to be vertical. NLC results differ sharply from ED, even with nonzero w, around $h = 0.6$. Whether the phase immediately to the left of the boundary is a true thermodynamic QSL or an inhomogeneous Griffiths-McCoy-like phase [40] with only pockets of high entanglement deserves further attention. The paramagnetic phase boundary at large w is roughly horizontal. Various properties collapse on a single scaling curve at larger w implying a predominantly local paramagnetic behavior. The confinement transitions due to randomness, obtained in the finite cluster study from Ising correlations and entanglement entropy, respectively, are shown by open and closed triangles. The thermodynamic phase boundary, where hexagonal loop resonances are lost, is shown by diamonds, and perturbation theory results are indicated by a dashed line. The nature of the phase transition and the possibility of a long-ranged spin-glass phase deserves further consideration [41].

IV. SUMMARY AND CONCLUSION

To summarize, we have studied the random transverse-field Ising model on the pyrochlore lattice using NLC and ED. This model has a deconfined QSL phase, which is subject to two types of confining transitions [32]. Large transverse fields lead to confinement where spins are locked along the field direction. On the other hand, a distribution of random fields leads to a selection within the ice manifold also leading to a loss of entanglement and confinement. We have shown that local entanglement associated with spins in a tetrahedron contains sharp changes associated with these transitions.

Simple NLC converges well in the high-field phase, right up to the transition. But it diverges in the QSL. The QSL phase can be studied within NLC by embedding each cluster inside a spin ice. Nearly all the entanglement in the QSL phase arises from ring-exchange resonances. These can be frozen by random transverse fields leading to confinement.

In the confining phase, there is a distribution of local entanglement entropies, a property that persists to large random fields. Experiments on $Pr_2Zr_2O_7$ found rather large randomness [33], implying that the system can at best have pockets

of high entanglement. Improvement in material preparation should lead to reduced disorder. Our work provides quantitative estimates of how much randomness needs to be lowered to obtain a true QSL phase.

It would be interesting to extend these studies to random XXZ and other models of quantum spin ice, where many other varieties of quantum spin-liquid phases are known to exist [42].

ACKNOWLEDGMENTS

We thank Z. Bai for helpful discussions. This work was performed under the auspices of the U.S. Department of Energy by Lawrence Livermore National Laboratory under Contract No. DE-AC52-07NA27344. Document release number LLNL-JRNL-778510. The work of RRPS is supported by NSF-DMR Grant No. 1855111.

[1] L. Balents, Nature (London) **464**, 199 (2010).
[2] L. Savary and L. Balents, Rep. Prog. Phys. **80**, 016502 (2017).
[3] T. H. Han, J. S. Helton, S. Y. Chu, D. G. Nocera, J. A. Rodriguez-Rivera, C. Broholm, and Y. S. Lee, Nature (London) **492**, 406 (2012); M. Fu, T. Imai, T.-H. Han, and Y. S. Lee, Science **350**, 655 (2015).
[4] Y. Shen, Y.-D. Li, H. Wo, Y. Li, S. Shen, B. Pan, Q. Wang, H. C. Walker, P. Steffens, M. Boehm, Y. Hao, D. L. Quintero-Castro, L. W. Harriger, M. D. Frontzek, L. Hao, S. Meng, Q. Zhang, G. Chen, and J. Zhao, Nature (London) **540**, 559 (2016); Y. D. Li, Y.-M. Lu, and G. Chen, Phys. Rev. B **96**, 054445 (2017); Z. Zhu, P. A. Maksimov, S. R. White, and A. L. Chernyshev, Phys. Rev. Lett. **120**, 207203 (2018).
[5] G. Jackeli and G. Khaliullin, Phys. Rev. Lett. **102**, 017205 (2009).
[6] J. G. Rau, EricKin-Ho Lee, and H.-Y. Kee, Phys. Rev. Lett. **112**, 077204 (2014); S. M. Winter, K. Riedl, D. Kaib, R. Coldea, and R. Valenti, *ibid.* **120**, 077203 (2018).
[7] A. Banerjee, C. A. Bridges, J.-Q. Yan, A. A. Aczel, L. Li, M. B. Stone, G. E. Granroth, M. D. Lumsden, Y. Yiu, J. Knolle, D. L. Kovrizhin, S. Bhattacharjee, R. Moessner, D. A. Tennant, D. G. Mandrus, and S. E. Nagler, Nat. Mater. **15**, 733 (2016).
[8] Y. Kasahara, T. Ohnishi, Y. Mizukami, O. Tanaka, S. Ma, K. Sugii, N. Kurita, H. Tanaka, J. Nasu, Y. Motome, T. Shibauchi, and Y. Matsuda, Nature (London) **559**, 227 (2018).
[9] I. Kimchi, A. Nahum, and T. Senthil, Phys. Rev. X **8**, 031028 (2018).
[10] Z. Zhu, P. A. Maksimov, S. R. White, and A. L. Chernyshev, Phys. Rev. Lett. **119**, 157201 (2017).
[11] J. Knolle, R. Moessner, and N. B. Perkins, Phys. Rev. Lett. **122**, 047202 (2019).
[12] K. Uematsu and H. Kawamura, Phys. Rev. B **98**, 134427 (2018).
[13] K. Uematsu and H. Kawamura, J. Phys. Soc. Jpn. **86**, 044704 (2017).
[14] E. C. Andrade, J. A. Hoyos, S. Rachel, and M. Vojta, Phys. Rev. Lett. **120**, 097204 (2018).
[15] R. R. P. Singh, Phys. Rev. Lett. **104**, 177203 (2010).
[16] I. Rousochatzakis, S. R. Manmana, A. M. Lauchli, B. Normand, and F. Mila, Phys. Rev. B **79**, 214415 (2009).
[17] M. J. P. Gingras, Spin ice, in *Introduction to Frustrated Magnetism*, edited by C. Lacroix, P. Mendels, and F. Mila (Springer-Verlag, Berlin, Heidelberg, 2011).
[18] A. P. Ramirez, A. Hayashi, R. J. Cava, R. Siddhartan, and B. S. Shastry, Nature (London) **399**, 333 (1999).
[19] K. A. Ross, L. Savary, B. D. Gaulin, and L. Balents, Phys. Rev. X **1**, 021002 (2011).
[20] L. Savary and L. Balents, Phys. Rev. Lett. **108**, 037202 (2012).
[21] M. Hermele, M. P. A. Fisher, and L. Balents, Phys. Rev. B **69**, 064404 (2004).
[22] A. H. Castro Neto, P. Pujol, and E. Fradkin, Phys. Rev. B **74**, 024302 (2006).
[23] N. Shannon, O. Sikora, F. Pollmann, K. Penc, and P. Fulde, Phys. Rev. Lett. **108**, 067204 (2012).
[24] A. Banerjee, S. V. Isakov, K. Damle, and Y. B. Kim, Phys. Rev. Lett. **100**, 047208 (2008).
[25] M. Taillefumier, O. Benton, H. Yan, L. D. C. Jaubert, and N. Shannon, Phys. Rev. X **7**, 041057 (2017).
[26] L. Pauling, J. Am. Chem. Soc. **57**, 2680 (1935).
[27] L. Savary and L. Balents, Phys. Rev. Lett. **118**, 087203 (2017).
[28] O. Benton, Phys. Rev. Lett. **121**, 037203 (2018).
[29] R. Moessner, S. L. Sondhi, and E. Fradkin, Phys. Rev. B **65**, 024504 (2001).
[30] J. Rochner, L. Balents, and K. P. Schmidt, Phys. Rev. B **94**, 201111(R) (2016).
[31] P. Emonts and S. Wessel, Phys. Rev. B **98**, 174433 (2018).
[32] G. Chen, Phys. Rev. B **94**, 205107 (2016).
[33] J.-J. Wen, S. M. Koohpayeh, K. A. Ross, B. A. Trump, T. M. McQueen, K. Kimura, S. Nakatsuji, Y. Qiu, D. M. Pajerowski, J. R. D. Copley, and C. L. Broholm, Phys. Rev. Lett. **118**, 107206 (2017).
[34] M. Rigol, T. Bryant, and R. R. P. Singh, Phys. Rev. Lett. **97**, 187202 (2006); Phys. Rev. E **75**, 061118 (2007).
[35] A. B. Kallin, K. Hyatt, R. R. P. Singh, and R. G. Melko, Phys. Rev. Lett. **110**, 135702 (2013).
[36] B. Tang, E. Khatami, and M. Rigol, Comput. Phys. Commun. **184**, 557 (2013).
[37] R. Applegate, N. R. Hayre, R. R. P. Singh, T. Lin, A. G. R. Day, and M. J. P. Gingras, Phys. Rev. Lett. **109**, 097205 (2012); N. R. Hayre, K. A. Ross, R. Applegate, T. Lin, R. R. P. Singh, B. D. Gaulin, and M. J. P. Gingras, Phys. Rev. B **87**, 184423 (2013).
[38] H. Changlani, arXiv:1710.02234.
[39] D. S. Rokhsar and S. A. Kivelson, Phys. Rev. Lett. **61**, 2376 (1988).
[40] R. B. Griffiths, Phys. Rev. Lett. **23**, 17 (1969); B. M. McCoy, Phys. Rev. **188**, 1014 (1969).
[41] A. Andreanov, J. T. Chalker, T. E. Saunders, and D. Sherrington, Phys. Rev. B **81**, 014406 (2010).
[42] O. Benton, L. D. C. Jaubert, R. R. P. Singh, J. Oitmaa, and N. Shannon, Phys. Rev. Lett. **121**, 067201 (2018).